Carbon 109 (2016) 331–339

Contents lists available at ScienceDirect

Carbon

journal homepage: www.elsevier.com/locate/carbon

Effect of graphene nano-platelet morphology on the elastic modulus of soft and hard biopolymers

Pietro Cataldi [a], Ilker S. Bayer [a, *], Gabriele Nanni [a], Athanassia Athanassiou [a], Francesco Bonaccorso [a], Vittorio Pellegrini [a], Antonio Esau del Rio Castillo [a], Filiberto Ricciardella [a], Sergey Artyukhin [a], Marc-Adrien Tronche [b], Yury Gogotsi [c], Roberto Cingolani [a]

[a] Istituto Italiano di Tecnologia, Via Morego 30, 16163, Genova, Italy
[b] École Nationale Supérieure de Chimie de Montpellier, 8 Rue de L'ecole Normale, 34090, Montpellier, France
[c] Department of Materials Science and Engineering, A.J. Drexel Nanomaterials Institute, Drexel University, 3141 Chestnut St, Philadelphia, PA, 19104, United States

ARTICLE INFO

Article history:
Received 13 June 2016
Received in revised form
8 August 2016
Accepted 10 August 2016
Available online 13 August 2016

ABSTRACT

Free-standing biocomposites were fabricated by solvent casting and hot-pressing employing two bio-polyesters having diverse elastic (Young's) moduli (soft and hard), reinforced with different graphene nanoplatelets (GnPs). Systematic mechanical measurements were conducted to investigate the effect of GnP thickness and lateral size on the elastic moduli. Comparisons were made with other reinforcing nanostructured filers such as organoclay, MoS_2, Fe_2O_3, carbon black and silica nanoparticles. Upon solvent casting, GnPs did not perform better than the other model fillers in increasing the elastic modulus of the soft bio-polyester. Upon hot-pressing however, large (>300 nm) multi-layer GnPs (≥8 layers) more than doubled the elastic modulus of the soft bio-polyester matrix compared to other GnPs and fillers. This effect was attributed to the optimized alignment of the large 2D GnP flakes within the amorphous soft polymer. In contrast, hot-pressing did not yield superior elastic modulus enhancement for the hard bio-polyester when hot-pressed. GnPs only induced 30% enhancement for both processes. Moreover, multi-layer large GnPs were shown to suppress the thermally-induced stiffness reduction of the soft bio-polyester near its melting temperature. A theoretical analysis based on the spring network model is deployed to describe the impact of the GnP alignment on the elastic moduli enhancement.

1. Introduction

Nanoscale hybrid materials made up of graphene bio-composites, demonstrate enormous research and development potential due to the fact that graphene can considerably enhance and even eliminate various drawbacks associated with bio-based polymers, rendering them next generation green composites [1–5]. However, as in the case of synthetic polymer-graphene composites, such new properties emerge only when graphene is well dispersed and in the form of single or few-layer flakes, which is quite challenging to maintain [6,7]. Nonetheless, multi-layer graphene (MLG) flakes, generally referred to as graphene nanoplatelets (GnPs) or exfoliated graphite flakes, with properties in between single layer graphene (SLG) and graphite, are being widely used to design polymer nanocomposites with many interesting properties [7–11]. This has been made possible by the recent developments in synthesizing GnPs in large scales [12,13]. Apart from their electrical properties, GnPs have been employed as reinforcing agents for tuning stiffness of polymers [5,14–16]. For instance, at low nanoscale filler contents GnPs were shown to perform significantly better than carbon nanotubes in terms of enhancing a variety of mechanical properties including tensile strength, elastic modulus, fracture toughness, fracture energy and resistance to fatigue and crack growth [17]. There are still many open fundamental issues related to interaction of graphene flakes with polymer matrices such as polymer-graphene interface interactions and segregation [18]. Review of literature indicates that the geometry of the GnPs is considered to be the key parameter for

* Corresponding author.
E-mail address: ilker.bayer@iit.it (I.S. Bayer).

http://dx.doi.org/10.1016/j.carbon.2016.08.026
0008-6223/

the elastic modulus enhancement and reinforcement [19]. For instance, it was shown that the 2D nature of the nanoflakes is the major reason for stiffening due to enhanced specific surface area of GnPs and improved mechanical interlocking/adhesion at the filler-matrix interface [17,20]. In particular, contradictory results (worsening or enhancing of elastic moduli) have been reported on the effect of the average lateral size and the thickness of the GnPs on the final mechanical properties of polymeric matrices [19,21,22]. Moreover, as a rule of thumb, elastic modulus of a reinforced polymer is strongly dependent on the degree of dispersion as well as directional alignment of the fillers inside the matrix [23]. For polymer-graphene composites, directional alignment of GnPs has been reported to favor enhanced mechanical properties [24,25]. Another important aspect is the chemical interfacial interactions between the polymeric matrix and the graphene flakes [26]. Several works reported that properly functionalized graphene flakes forming strong chemical interactions with the polymer results in favorable reinforcing effect on the elastic modulus [17,27–29]. However, it is still very difficult to single out effects of geometry, alignment and chemistry of the GnPs from one another during the interpretation of elastic modulus changes in polymer-GnP composites. This is further complicated by the type of polymer matrix to be used like thermoplastic or thermosetting, crystalline, semi-crystalline or amorphous polymers [30–32].

In the case of thermoplastic polymers and biopolymers, non-conductive graphene oxide (GO) [33,34] has been used extensively to fabricate nanocomposites particularly with water soluble biopolymers [5,8,35–43]. In most cases, nanocomposites in the form of hydrogels for biomedical applications were developed utilizing GO or reduced graphene oxide (RGO) [35,36,40,42]. On the other hand, there are various promising polyester-based biopolymers that have been developed with the aim to replace certain oil based polyesters [44–47]. Among them, polylactic acid (PLA) and polycaprolactone (PCL) have been industrialized [48]. Interaction of various forms of graphene-based materials (e.g., GO, RGO etc.) with these polymers has been recently considered important due to the fact that graphene as an additive could reduce or eliminate many drawbacks associated with these bio-polyesters such as poor thermal properties, unacceptably low levels stiffness and poor water and gas barrier properties [31,48]. So far, little attention has been paid towards the comparative aspects of using various forms of GnPs in thermoplastic linear chain bio-polyesters processed by thermoforming.

Hence, the aim of this study is to investigate the effect of size and geometry of various GnPs on the elastic modulus of two industrially important types of bio-polyesters, namely, Mater-Bi® (soft matrix) and PLA (hard matrix). Systematic comparative measurements were also carried out with other 2D and 3D nanoscale additives such as organoclays (nanoclay), molybdenum disulfide (MoS_2), carbon black (CB), nano-silica (SiO_2) and iron oxide (Fe_2O_3) in order to distinguish and differentiate the real effect of GnPs on the elastic moduli of the two types of biopolymers. Our experimental results are also corroborated from the theoretical point of view with the nanocomposite polymer reinforcement modeled using a spring-net model under uniaxial load [49]. The strain fields inside the matrix and the effective elastic moduli are calculated and compared to the experimental data. The calculations provide a microscopic illustration for the observed polymer reinforcement and allow rationalizing the results. Moreover, for the soft bio-polyester matrix, the reduction of the elastic modulus due to heating near melting point is considerably reduced by the presence of GnPs with a large lateral size.

2. Experimental section

2.1. Preparation of GnPs

Fabrication of G 3-130 flakes: The graphite flakes (+100 mesh, ≥75% min) and N-Methyl2pirrolidone (NMP) (99.5% purity) were purchased by Sigma-Aldrich and used without further purification. We exploited the liquid phase exfoliation (LPE) of graphite to produce the graphene inks in NMP. For this scope 10 g of graphite flakes was dispersed in 1000 ml of NMP and ultrasonic processed (VWR®) for 6 h. The resulting dispersion was then ultra-centrifuged at ~16000 g in a Beckman Coulter Optima™ XE-90 (SW32Ti rotor) and exploiting sedimentation-based separation we removed the thick flakes and un-exfoliated graphite [50–52]. Afterward, we collected the 90% of the supernatant by pipetting. Subsequently, the as-obtained dispersion is dried using a rotary evaporator (Heidolph® mod. HeiVap Presition MLG6) set at 70 °C and a vacuum of 2mBar obtaining a powder.

Fabrication of G 3-120 flakes: 10 g of graphite flakes was dispersed in 1000 mL of NMP and ultrasonic processed (VWR®) for 6 h. The resulting dispersion was then successively ultrasonic processed for another hour by using a sonic tip (Branson digital sonifier) adjusted at 45% power. The suspension is let to decant overnight and the 70% of the supernatant is pipetted. Afterwards the as-produced dispersion is dried using a rotary evaporator (Heidolph® mod. HeiVap Presition MLG6) set at 70 °C and a vacuum of 2mBar obtaining a powder.

G 9-410 flakes were purchased from Strem Chemicals (product number 06-0210). G 21-340 and G 8-600 were donated by Directa Plus (respectively grade Ultra G+ and Pure G+). Fabrication details of G 6-50 flakes are given elsewhere [53]. Carbon Black from Cabot grade N330 was donated by Directa Plus. Iron(III) oxide (powder, product number 310050) was acquired from Sigma-Aldrich. Fumed hydrophobic silica nanoparticles (Aerosil R812; 230–290 m^2/g, BET) were purchased from Evonik Inc. Molibdenum(IV) sulfide (powder, product number 234842) was ordered by Sigma-Aldrich. Nanoclay, surface modified containing 0.5–5 wt% amino-propyltriethoxysilane and 15–35 wt% octadecylamine was obtained by Sigma-Aldrich (product number 682632). Mater-Bi® bioplastic (grade Z) is a product of Novamont S.p.A, Italy. PLA was purchased from Nature works LLC Company (Ingeo™ Biopolymer 2003D). Chloroform was acquired from Sigma-Aldrich. It was employed to dissolve the biopolymers. 0.625 g of bioplastics was used for the solvent cast films. The amount of chloroform was different for the MB and the PLA matrixes. We employed 5 ml for the first biopolymer and 10 for the second. These parameters were fixed taking into account the viscosity of the obtained solution. In fact, viscosity is a key parameter to ensure a good dispersion when the fillers were added and mixed by tip-sonication (750 W, 40% amplitude, 20 kHz, six-eight times for 15 s using a Sonics & Materials, Inc. Model Num. VCX750) and drop cast in Teflon petri dishes (7.5 cm diameter). Note that when the polymer-GnP solutions were prepared they were sonicated for a short duration (15 s) in order to enable dispersion in solution. This is not expected to create any significant defect in the GnPs however some flakes can break down into smaller ones which is reflected in the final lateral size distribution that is used to identify different fillers. The resultant solution with PLA biopolymer was more viscous therefore we employed more chloroform. To prepare the hot pressed samples, all the solid and solvent quantities were doubled (1.25 g of bio-polyesters, 10 ml and 20 ml of $CHCl_3$ respectively for the Mater-Bi® and PLA solution). In this way, both solvent cast and hot pressed samples had a thickness of approximately 100 μm. After drying

overnight, the films were placed in an oven at 120 °C for 4 h to ensure complete solvent evaporation. The solvent cast samples were then ready for measurements (see Fig. 1). For the hot pressed ones another step was needed: The samples were pressed (15 bar) for 4 min at a temperature of 175 °C. For each kind of filler and concentration minimum of five samples were tested. Non-stick Teflon films (Advent Research Materials, Art. Num. FP823338) were used during the hot-pressing process to prevent possible sticking of the composites on the surfaces of the press. The hot-pressing was performed using a Specac-Atlas Power Presses T8 or a Specac-Atlas 15T Manual Hydraulic press. All samples contained 0.1, 1, 3 and 5 wt% fillers on dry basis.

2.2. Mechanical characterization

To determine the Young's Modulus, a tensile tester (Instron 3365) was used. Samples were stretched by applying a strain rate of 1 mm min^{-1} for PLA and 10 mm min^{-1} for Mater-Bi®. Elastic (Young's) moduli of the pure PLA and Mater-Bi® matrix produced with the two fabrication methods are reported in Table S1. The Young's moduli of the samples were experimentally determined from the slope of stress–strain curves obtained during tensile tests. 1% and 0.5% of strain were imposed in the case of soft and hard matrix, respectively. The extension rate was 0.5 mm min^{-1}, with a gauge length of 10 mm. Before the tensile test, the samples were heated up for 3 min on a digital hotplate set at the desired temperature. In all cases, at least three samples were tested from which the mean and standard deviation were calculated. A micrometer from Mitutoyo (series 293) was utilized to determine thicknesses of samples.

2.3. Electron microscopy: transmission electron microscopy (TEM) and scanning electron microscopy (SEM)

The morphology of the 2D and 3D fillers used in this study were analysed by TEM (JOEL JEM 1011 instrument with an acceleration voltage of 100 kV). For this study, the samples were dispersed in NMP and 20 μL dropped on copper grids (200 mesh), which were then dried under vacuum overnight. The statistical analysis of the lateral sizes was based on measurements on 150 flakes using Image-J software. For details refer to the Supporting Information (Figs. S1 & S2). High-resolution scanning electron microscopy (SEM) imaging was carried out using a JEOL JSM 7500FA equipped with a cold FEG and a JEOL microscope (model JSM-6490LA). Both microscopes were operated at an acceleration voltage of 15 kV. The fillers for SEM images were drop cast from a dilute solution (0.02 mg/ml) respectively on silicon plates or on TEM grids. The thicknesses of the MoS_2 were estimated using the scanning electron SEM images employed in Fig. S2, making a statistic on the flakes disposed vertically. In Fig. S3 is shown a representative high resolution SEM image of the thickness of the MoS_2 flakes. It is measured as 95 ± 40 nm. Regarding organoclay (nanoclay), the single flakes present a nominal thickness indicated by the producer of 1 nm. However, we estimate the final thickness inside the composite to be of the same order of magnitude of MoS_2.

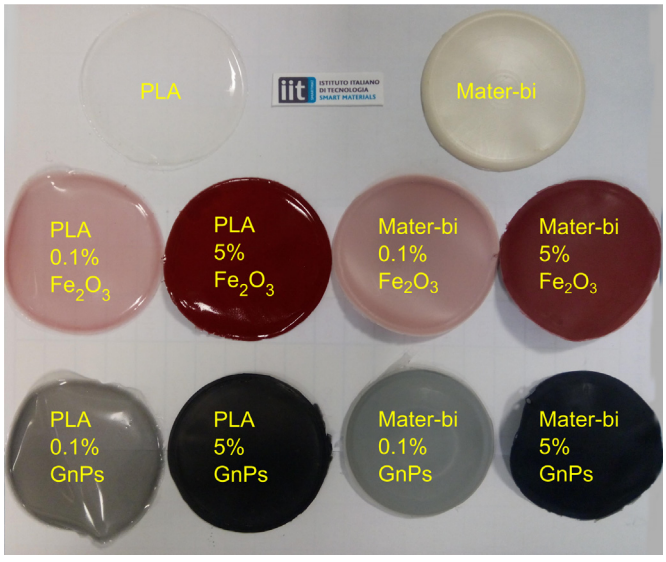

Fig. 1. Photograph of different solvent-cast composite films from PLA and Mater-Bi® biopolymers. Transparent and whitish films featured on the top are two unfilled matrices. (A colour version of this figure can be viewed online.)

2.4. Atomic force microscopy (AFM)

Atomic force microscopy (AFM) measurements were carried out at room temperature and air atmosphere using an Innova AFM (Bruker, Santa Barbara, CA), set in tapping mode, with a NTESPA 3.75 mm cantilever (Bruker, 300 kHz k: 40 N m^{-1}). The analysis software used was Gwyddion version 2.43. The analysed samples have a large distribution of thicknesses ranging from SLG to few layers (FLG) (1–4 layers, or 1–4 nm), to graphite (more than 8 layers). The AFM statistic was carried out on measurements on 30 flakes per sample. The thickness distribution fitting is obtained by using the Log-normal distribution. The thickness results are summarized in Table 1. The AFM topological images are shown in Fig. S4, additionally their respective thickness distributions are also given.

2.5. Raman spectroscopy

Raman measurements were carried out with a Renishaw 1000 at 532 nm excitation wavelength and a 100× objective, with an incident power of ≈1 mW. The D, G, and 2D peaks were fitted with Lorentzian functions. The Raman spectra of the four samples and graphite are shown in Fig. S5a.

The Raman spectra of the graphene and graphite–like materials were analysed and the details and the relevant discussion are given in the Supporting Information. The sub-components of the 2D band $2D_1$, and $2D_2$ (see Fig S5b) are used to evaluate the quality of the graphitic flakes, in term of number of layers, which were in agreement with the AFM data reported in Section S2.3.

2.6. Thermo-mechanical measurements

The results regarding the thermal stability of both the Mater-Bi® and PLA films with G 8-600 were investigated using thermogravimetric analysis (TGA) and reported in Fig. S6. TGA was conducted using a TA instruments apparatus (model Q500, from room temperature to 600 °C in nitrogen environment). Further details are presented and discussed in the Supporting Information referring to Fig. S6.

2.7. Polymer crystallinity measurements with X-ray diffraction

The crystal structure was measured with X-ray diffraction (XRD) employing a Rigaku SmartLab X-Ray diffractometer, provided with a 9 kW Cu Kα (λ = 1.542 Å) rotating anode, running at 40 kV and 150 mA. A Göbel mirror was utilized to convert the divergent X-ray beam into a parallel beam and to eliminate the Cu Kβ radiation (λ = 1.392 Å). The diffraction patterns were acquired at ambient and high temperatures, over an angular range of 7.5°–50° for the PLA,

Table 1
Tabulated list of nanoscale filler materials used and their average size and thickness values. For GnPs, a notation in the form of G *t-L* is used, in which *t* stands for thickness and *L* the lateral size. For instance, G 9-410 indicates GnP flakes with 9 nm thickness and 410 nm lateral size, respectively.

Designation	Material[a]	Thickness (nm)	Lateral size (nm)	Number of layers	Diameter (nm)
G 21-340	Graphene	21	340	>8	n.a.
G 8-600	Graphene	8	600	>8	n.a.
G 9-410	Graphene	9	410	>8	n.a.
G 6-50	Graphene	6	50	>8	n.a.
G 3-130	Graphene	3	130	<8	n.a.
G 3-120	Graphene	3	120	<8	n.a.
CB	Carbon black	n.a.	n.a.	n.a.	35
SiO_2	Hydrophobic silica	n.a.	n.a.	n.a.	9
Fe_2O_3	Iron(III) oxide	n.a.	n.a.	n.a.	350
MoS_2	Molybdenum disulfide	95	1000	>8	n.a.
Clay	Montmorillonite	100	2000	>8	n.a.

[a] Although "Graphene" is used for all G t-L additives for simplicity, G21-340, G8-600, G9-410 are GnPs, G6-50 is MLG, and G3-130 and G3-120 are FLG samples, respectively.

and 7°–60° for Mater-Bi® with a step size of 0.05° and scan rate 1.2°/min. We performed X-ray diffraction measurements of composites made with Mater-Bi® and PLA and we reported the results in Fig. S7.

3. Results and discussion

The two representative biopolymers employed in this study are bio-polyesters having significantly different elastic moduli. Mater-Bi® has a Young's modulus of ~100 MPa [54,55], whereas PLA of ~2 GPa [56–59]. In order to investigate the effect of GnP geometry, size and orientation on the stiffening of these two polymer matrices, six different types of commercial and in-house synthesized GnPs were used. No post-chemical functionalization or oxidation of the GnPs was made. The lateral size, thickness and approximate number of layers of each GnP were characterized by using a combination of SEM/TEM statistical imaging, Raman spectroscopy and AFM (see Figs. S1–S5). To simulate melt processing, solvent cast biopolymer-GnP films were hot pressed (175 °C, 15 kPa, ½ hours). We chose this temperature to ensure melting of both polymers during pressing without thermally degrading them (see Fig. S6). Since hot-pressing process can cause orientation of the fillers in the melted polymer matrix [60], it can allow comparisons with randomly dispersed films obtained by only solvent casting. Note that elastic modulus of certain polymers can change due to thermal or melt processing as their crystallinity is modified [61,62]. In order to ensure that the observed variations in elastic modulus are only due to GnPs rather than hot-pressing conditions, Young's moduli of both polymers after solvent casting alone and followed by hot-pressing were measured. Elastic modulus of Mater-Bi® remained the same whereas PLA's decreased slightly from 2.1 GPa to 1.9 GPa (see Table S1) as a result of hot-pressing. We attributed these variations to the changes in the crystallinity of PLA (see Fig. S7) [61,62]. Table 1 shows morphological data of all the nanoscale materials used in this study. As listed, measurements indicate that for the GnPs, flake thickness varied from 3 nm to 21 nm, whereas the lateral flake size was in the range from 50 nm to 600 nm. Other 2D fillers, namely, organoclay and MoS_2 were found to have thicknesses close to 100 nm, with lateral sizes of 1 μm and 2 μm, respectively. The nanoparticles, on the other hand, had varying diameters such as 9 nm for silica, 35 nm for carbon black and 350 nm for Fe_2O_3. Fig. 2 displays changes in the elastic moduli of the solvent cast soft and hard bio-polyester nanocomposites as a function of filler weight percent that ranged from 0.1 wt% to 5.0 wt %. In the case of the soft matrix (Mater-Bi® in Fig. 2a), as a general trend, increasing filler concentration increased the elastic modulus. For certain fillers such as carbon black, silica and G 21–340, this enhancement reached approximately 170 MPa at 5.0 wt% levels, corresponding to a 65% improvement.

However, Fig. 2a indicates that regardless of the concentration levels studied, no superior effect of GnPs on stiffening the polymer matrix was measured over other fillers. In the case of hard matrix (PLA), GnP flakes were more effective in increasing the elastic modulus beyond 1.0 wt % as seen in Fig. 2b. This was true for large multi-layer GnPs as well as few-layer ones (only two are exemplified for clarity in the plot). For instance, both few-layer (G 3-130) and multi-layer (G 8-600) flakes stiffen the PLA matrix compared to others. As such, the elastic modulus of solvent cast PLA films can be increased up to 2.7 GPa (~30% increase) by inclusion of GnPs. In the case of carbon black and MoS_2 particles, the elastic modulus of filled PLA remained practically unaltered within the concertation range studied. Clearly, in order for GnPs to act as effective elastic modulus enhancers in a bio-polyester matrix, not only the size, thickness and chemistry of graphene (oxidation, functionalization, etc.) matter, but also the original elastic modulus of the biopolymer, particularly for solvent processed films. Strength of interactions between the particles and the polymer matrix is critical for stress transfer to the reinforcing particles and achieving improved mechanical properties [63].

Next, we present the cases for both soft and hard biopolymer composites fabricated by hot pressing, after solvent casting. Detailed transmission electron microscopy (TEM) studies indicated that upon hot pressing, GnPs align within the bio-polyester matrices; particularly in the amorphous Mater-Bi® matrix as shown and indicated by the arrows in Fig. 3.

In order to facilitate interpretation of the measurements, the data were collected and grouped as 2D (all GnPs, MoS_2, organoclay) and 3D (carbon black, silica, iron oxide) fillers for both the soft (Fig. 4a and b) and the hard (Fig. 4c and d) biopolymer matrices. In the case of Mater-Bi® matrix, significant differences are obtained in elastic modulus changes as a function of 2D filler type as well the morphological attributes of GnPs. Inspection of Fig. 4a indicates that large multi-layer GnPs considerably enhance Mater-Bi® elastic modulus up to 200%. Few-layer graphene flakes, on the other hand, triggered an approximate 100% enhancement in elastic modulus of Mater-Bi®. These were GnPs identified as G 3-120, G 3-130 and G 6-50. The trends regarding other 2D particles, namely clay and MoS_2, show that they produced only about a 50% improvement in elastic modulus of the polymer, four-five times less than large GnPs, such as the particles identified as G 9-410.

Results pertaining to the effect of 3D nano-fillers (nanoparticles) on the elastic modulus of Mater-Bi® are summarized in Fig. 4b. Clearly, the overall trend is that the type of the nanoparticle does not play a role in enhancing the elastic modulus of Mater-Bi®, considering the uncertainties associated with the measurements. It can be stated that the nanoparticles employed in this study cause only about 20% enhancement in the elastic modulus of the soft biopolymer matrix under hot-pressing. This can be attributed to the

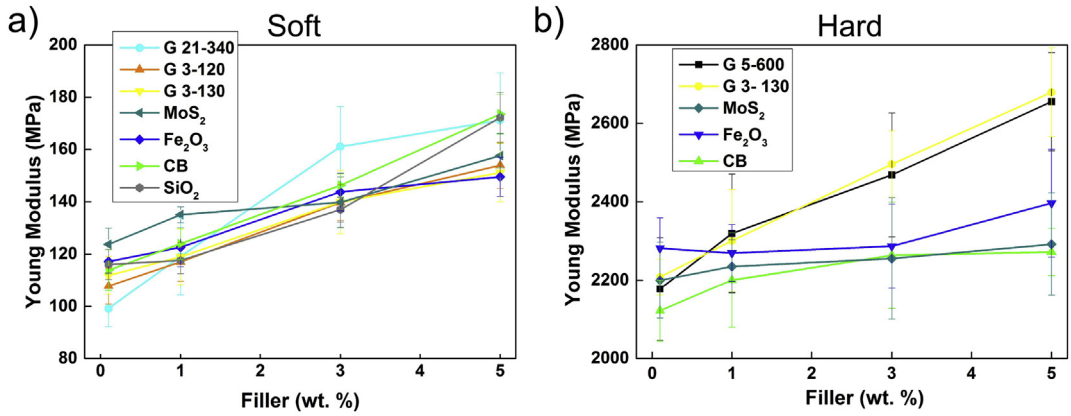

Fig. 2. Elastic modulus versus filler weight percent measurements for solvent-cast (a) soft (Mater-Bi®) and (b) hard (PLA) polymer matrix composites. (A colour version of this figure can be viewed online.)

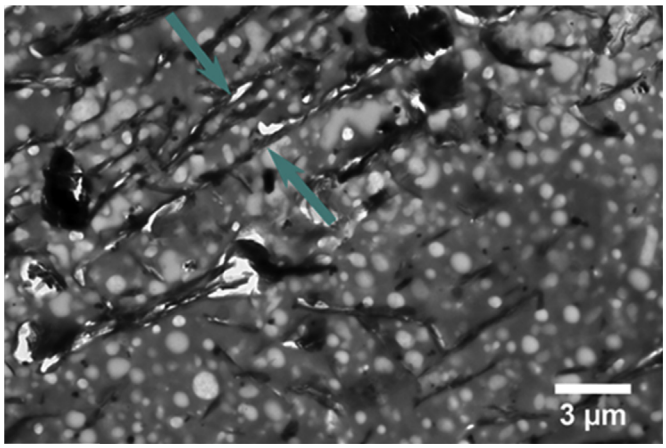

Fig. 3. Cross-section TEM image of hot pressed Mater-Bi® sample filled with G 8-600 GnPs The green arrows indicate GnPs that seem to have aligned due to hot-pressing. The white spots are thermoplastic starch particles originating from the soft matrix. (A colour version of this figure can be viewed online.)

presence of nanoparticle agglomerations due to electrostatic interactions, when concentration levels in the polymer matrix exceed 1 wt% [64,65]. As such, stiffness of soft bio-polyesters can be effectively tuned and increased by multi-layer large GnP flakes instead of nanoparticles.

In the case of the hard bio-polyester matrix, hot-pressed PLA, identical set of measurements were carried out, the results of which are given in Fig. 4c and d. Inspection of Fig. 4c reveals that non-graphitic 2D particles, i.e., clay and MoS_2 do not trigger noticeable stiffness enhancements in the elastic modulus of PLA matrix. On the other hand, just like in the case of soft matrix, large multi-layer GnPs increase the elastic modulus of the hard biopolymer matrix but only by about 35%. This is an augmentation in stiffness that is an order of magnitude less than Mater-Bi® reported in Fig. 4a. Few-layer GnPs cause very limited enhancements in the elastic modulus of PLA not exceeding 17%. Although in terms of trends, both large multi- and few-layer GnP inclusions result in elastic moduli enhancements in the bio-polyesters under hot-pressing, the significant difference in augmentation of stiffness between Mater-Bi® and PLA can be due to the semi-crystallinity and inherent stiffness of PLA polymer chains that tend to impede polymer chain mobility, limiting GnP orientation within the matrix [31,66].

It is worth mentioning that further increase in the elastic modulus in PLA may be possible with further chemical functionalization of the GnPs used in this study [67]. The reported results, however, are found to be in agreement with other PLA-graphene composites prepared by *in-situ* reduction of GO [31]. Note also that in the case of PLA-GnP nanocomposites, hot-pressing process does not seem to introduce an extra overall enhancement in the elastic modulus compared to solvent casting (compare Figs. 2b and 4c). In both cases, the maximum elastic moduli obtainable are approximately 2.7 GPa. This could be attributed to the above mentioned crystallization differences between PLA and Mater-Bi®. Still, this requires a more in depth study that is beyond the scope of the current work. Finally, results reported in Fig. 4d indicate that in the case of nanoparticles, for all practical purposes, the hot-pressing process does not inflict any significant effect on the elastic modulus of PLA, for the concentration ranges studied herein. On average, all nanoparticles would bring about a stiffness enhancement close to 8% in its elastic modulus.

Hence, based on the results reported in Figs. 2 and 4, one can argue that for soft bio-polyester matrices reinforced with GnPs, elastic or Young's modulus enhancement is much better achieved with the hot-pressing method. This trend can be explained by the easier orientation and the alignment of the 2D flakes inside the amorphous polymer matrix, which is uniaxially compressed and sheared due to simultaneous heat and pressure application, as shown in Fig. 3. Under hot-pressing, loose and randomly coiled chains of amorphous polymers soften and move easier than semi-crystalline polymer segments. It can also be argued that GnPs with larger lateral sizes can easily align parallel to the plane of hot-pressing, causing higher elastic modulus values (yellow groups of Fig. 4a and c). This effect is practically impossible to obtain as a result of solvent evaporation-induced self-assembly within the polymer-GnP composites or by simple mixing into liquid resins [68].

In order to rationalize the experimental results, we have simulated the elastic modulus and the strain field within a matrix using a spring network model [49]. The model is also known as the lattice spring model (LSM) in which solids are modeled by a collection of springs connected at nodes which are distributed on a cubic lattice and hence the name. The main element of such models is the existence of a linear spring which exerts forces at the nodes located at its endpoints in order to keep the initial length constant. Such a simple model is sufficient to simulate an isotropic homogeneous elastic medium with a specific Poisson ratio. Other Poisson ratio values can be obtained by adding angular springs between adjoining linear springs which tend to restore the initial angle between them. Moreover, concepts such as the one of elastic

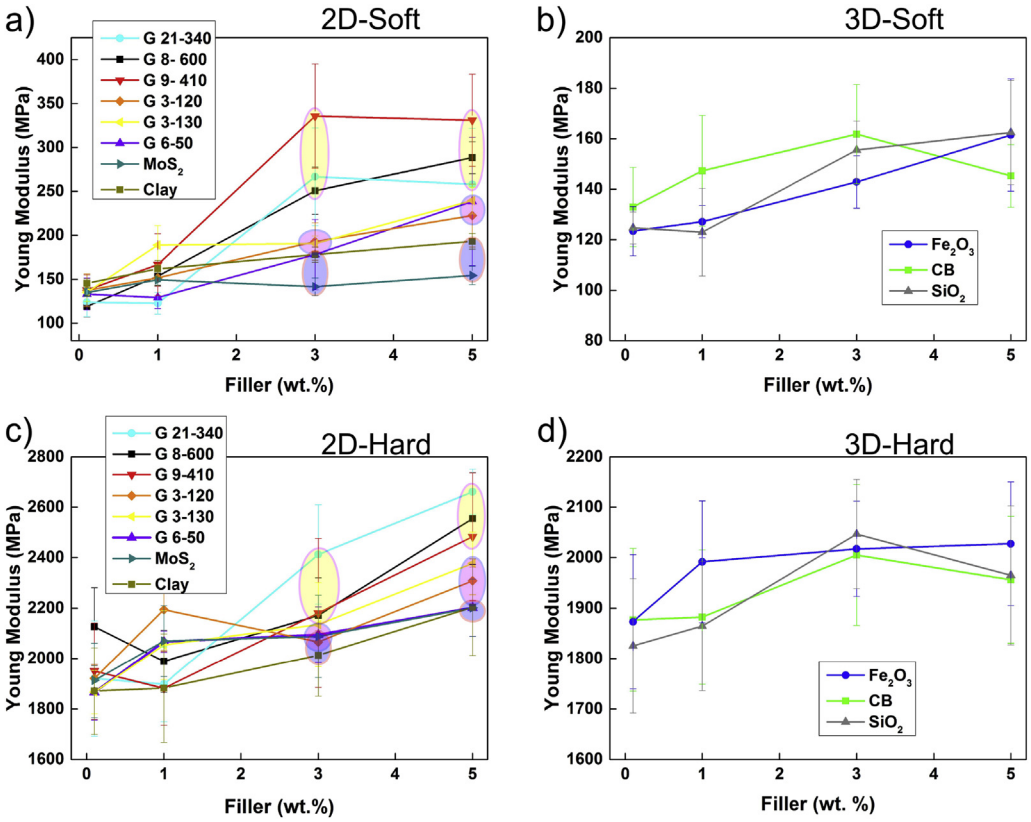

Fig. 4. Elastic modulus versus filler concentration plots for hot-pressed samples. Concentrations are given in weight percent. In (a), the plot shows elastic modulus measurements for all 2D fillers in Mater-Bi® matrix. In (b), the plot shows elastic modulus measurements for all 3D fillers in Mater-Bi® matrix. In (c), the plot shows elastic modulus measurements for all 2D fillers in PLA matrix and in (d) the plot shows elastic modulus measurements for all 3D fillers in PLA matrix. (A colour version of this figure can be viewed online.)

element can be included in order to improve the accuracy of the LSM [49]. Herein, this method does not take into account polymer chain mobility due to amorphous or crystalline polymer morphology. Cubic grids with 20^3 and 40^3 cells were used in calculations and the finite size effects were established to be small. The examples of simulated filler particle configurations and calculated strain fields are shown in Fig. 5a–c. Fig. 5a displays a matrix volume element with randomly oriented planar particles. Fig. 5b shows planar particles aligned in the *bc*-plane, while Fig. 5c presents cylindrical particles, with the diameter to height ratio of the order of one (3D particles). 3D particles were simulated as cylinders with the diameter similar to the height (based on the experimental data reported in Table 1), while planar flakes of layered materials were simulated as cylinders with a small height to diameter ratio identical to the values reported in Table 1 and the Supporting information. Solvent cast situation was simulated using randomly oriented planar particles, while hot pressing was modeled by particle alignment in the plane, in which the load was applied.

The positions of particles were chosen randomly within the simulated volume. The points at the boundary planes, where the load was applied, were assumed to be rigidly glued to the rigid plates and only moving along the loading force direction. The springs within the particle volume were assumed to have stiffness 1000 times larger than those outside. Fig. 5d shows the dependence of the effective elastic (Young's) modulus, E, on the filler volume fraction. The Young's modulus of the bare matrix is denoted as E_0. 240 randomly generated configurations were used to average over the particle distribution. On average, the samples with 2D particles have a larger Young's modulus than the samples with 3D particles. The alignment of 2D particles leads to a further increase of Young's modulus, confirming that this parameter is crucial for mechanical reinforcement of a polymer matrix with graphene 2D flakes. The 2D particles, extending along the loading force, shunt strain from the polymer matrix, thus providing the reinforcement [69]. At higher filler concentrations, “chains” of these particles, connecting the loading plates, are capable of shunting most of the strain from the polymer matrix, resulting in a super linear growth of Young modulus with particle concentration [69]. On the other hand, 2D particles oriented perpendicular to the loading force do not shunt any strain, and therefore do not lead to stiffness increase [69]. Thus, anisotropy of mechanical properties results from addition of preferentially oriented GnPs. The sample with randomly oriented 2D particles contains both “useful” particles, as well as the ones mostly perpendicular to the force, and therefore the reinforcement effects average out and exceed those of 3D particles of the same volume only marginally, as seen in Fig. 5d.

Note that as a result of computations shown in Fig. 5d, a 30% enhancement in elastic modulus can be estimated in the case 2D aligned particles. This value better approximates elastic modulus measurements of hard PLA matrix containing multi-layer GnP inclusions as shown in both Figs. 2b and 4c. This can be attributed to the fact that simulation does not account for rearrangements or self-assembly within the computational matrix, which better approximates the semi-crystallinity of PLA. Moreover, randomly distributed 2D fillers and the 3D fillers only cause about 15% enhancement in the elastic modulus. This number appears to match the experimental measurements corresponding to the amorphous soft bio-polyester matrix, Mater-Bi®, depicted in Fig. 4b.

Finally, effect of GnPs on the temperature dependent elastic

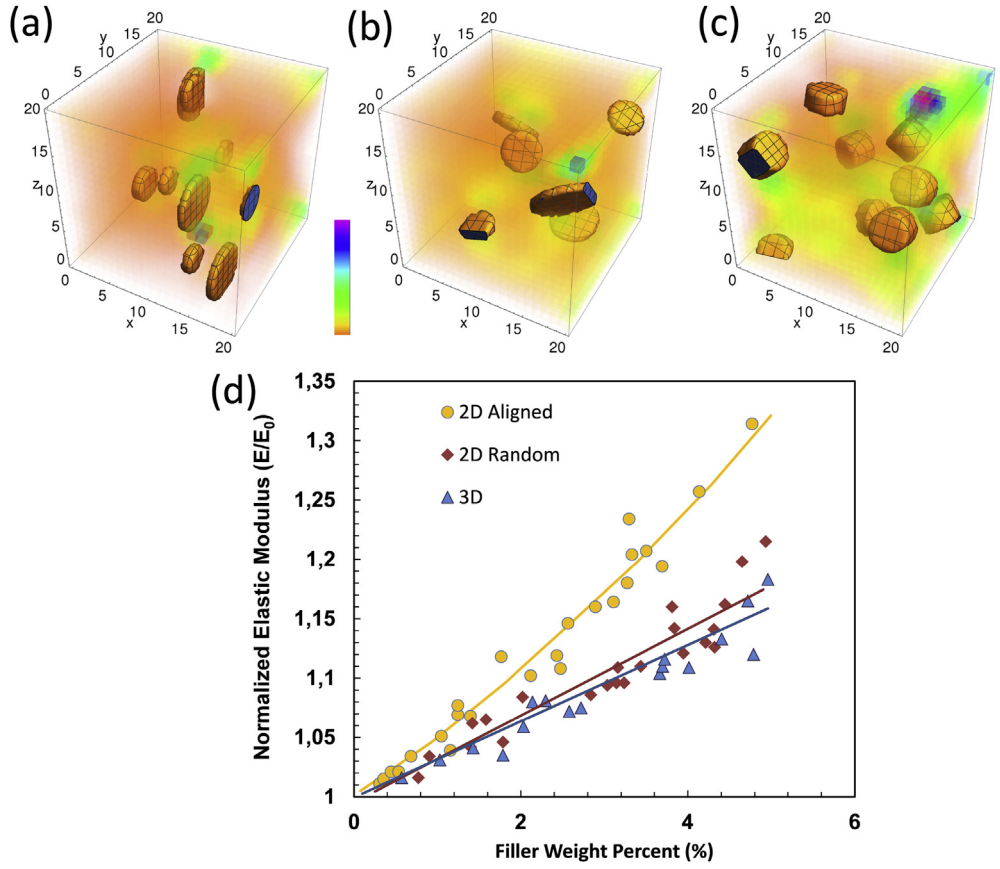

Fig. 5. Numerical simulations of elastic properties of filled polymers: stress energy density inside the filled polymer matrix is encoded in the color. (a) 2D flakes aligned in the same plane, (b) randomly oriented 2D flakes as a filler and (c) 3D particles. (d) Polymer matrix reinforcement: the Young modulus enhancement E/E_0 as a function of the filler weight percent. On average, the orange dots corresponding to aligned 2D flakes show a larger value of the E/E_0 ratio. Lines are displayed to guide the eye. (A colour version of this figure can be viewed online.)

modulus changes in bio-polyester matrices was investigated at 5.0 wt% concentration. Fig. 6a illustrates the changes in the elastic modulus that take place in the soft matrix and its composites over a range of temperatures that span from 25 to 50 °C. As seen in Fig. 6a, the elastic modulus of the matrix and the composites decreases with increasing temperature towards its melting point. The drop in the elastic modulus is related to the tendency of the polymer chains to slip off each other at higher temperatures [70]. An increase in temperature favors higher chain segments mobility and a decrease of the elastic modulus [71,72]. However, the slipping of the polymer chains under stress can be inhibited by anchoring the chains [73]. The enhanced thermo-mechanical properties are believed to arise from the strong interaction between graphene and the matrix, and the large steric hindrance of the graphene flakes. The graphene flakes act as anchor points and prevent the chains from slipping. In particular, the larger the in-plane dimension of the graphene flakes, the smaller the decrease of Young's modulus with the temperature. For example, with G 21-340, the elastic modulus of the composite decreased by 14% at 50 °C, while the modulus of the composite with graphene G 3-130 decreased by 25%. Moreover, the soft matrix and

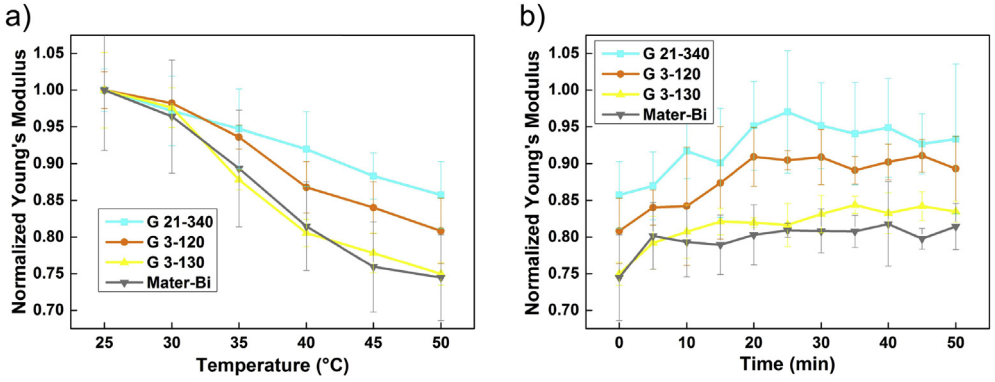

Fig. 6. Heating induced changes in the (normalized) elastic modulus of Mater-Bi® GnP composites before melting. In (a), larger lateral size GnPs cause less decline in elastic modulus. Similarly, in (b) upon cooling the composites with larger lateral size GnPs seem to recover their original elastic modulus. (A colour version of this figure can be viewed online.)

the composites displayed a memory effect for the non-stretched state, and tend to recover their original elastic modulus with time as shown in Fig. 6b. Similar tests were performed with PLA-based composites. In this case, the Young's modulus of the composite was substantially unaltered (see Fig. S8), probably due to the highly crystalline phase of the matrix and the range of temperatures used that is far from the melting temperature of PLA [59].

4. Conclusions

In summary, nanoscale biocomposites were fabricated by dispersing different graphene nanoplatelets (GnPs) as well as other non-graphitic 2D and 3D nanoscale particles in two representative bio-polyesters classified as soft and hard matrices. Films were produced by solvent casting and hot-pressing. Hot-pressing was found to align the GnPs within the polymer matrices. The alignment has more significant effect on the amorphous soft bio-polyester. The following observations were made: In the case of solvent cast soft matrix biocomposites, GnPs did not induce any superior enhancements in elastic moduli compared to other non-graphitic 2D and 3D fillers. In the case of the hard matrix, however, both large multi- and few-layer GnPs caused up to 35% increase in elastic modulus compared to other model 2D or 3D fillers. As a result of hot-pressing, GnP flakes significantly increased the elastic modulus of the soft bio-polyester. In particular, large multi-layer GnPs induced up to 200% stiffness enhancement compared to few-layer GnPs and non-graphitic 2D fillers. Upon hot-pressing, about 15% stiffness enhancement levels were measured in the nanoparticle filled soft bio-polyester. Compared to solvent casting, hot-pressing of the PLA matrix nanocomposites did not yield better elastic modulus enhancements neither by large multi- or few-layer GnPs. Stiffening levels remained the same. A theoretical analysis of the polymer/GnP composites based on the spring network model closely described the enhancement levels achieved in the hard bio-polyester. However, it could not predict the superior stiffening results due to large multi-layer GnPs measured for the soft bio-polyester. Moreover, large GnPs were shown to effectively suppress heat induced deterioration of the stiffness of the soft bio-polyester close to its melting temperature. These nanocomposites eventually recovered their initial elastic modulus upon cooling due to large multi-layer GnP inclusion. The results of this study indicate that GnPs can be promising next-generation candidates for elastic modulus engineering of soft amorphous biopolymers and their composites.

Acknowledgments

The authors acknowledge support from Drs. Massimiliano Bianchi and Laura Rizzi of DIRECTA PLUS S.p.a., Italy. The authors also acknowledge Alice Scarpellini for Electron Microscopy analysis and funding from the European Union's Horizon 2020 research and innovation program under grant agreement No. 696656 – GrapheneCore1.

Appendix A. Supplementary data

Supplementary data related to this article can be found at http://dx.doi.org/10.1016/j.carbon.2016.08.026.

References

[1] C. Wan, B. Chen, Poly (-caprolactone)/graphene oxide biocomposites: mechanical properties and bioactivity, Biomed. Mater. 6 (5) (2011) 055010.
[2] R. Li, C. Liu, J. Ma, Studies on the properties of graphene oxide-reinforced starch biocomposites, Carbohydr. Polym. 84 (1) (2011) 631–637.
[3] S. Sayyar, E. Murray, B.C. Thompson, S. Gambhir, D.L. Officer, G.G. Wallace, Covalently linked biocompatible graphene/polycaprolactone composites for tissue engineering, Carbon 52 (2013) 296–304.
[4] V. Mittal, A.U. Chaudhry, G.E. Luckachan, Biopolymer–thermally reduced graphene nanocomposites: structural characterization and properties, Mater. Chem. Phys. 147 (1) (2014) 319–332.
[5] J.R. Potts, D.R. Dreyer, C.W. Bielawski, R.S. Ruoff, Graphene-based polymer nanocomposites, Polymer 52 (1) (2011) 5–25.
[6] A.C. Ferrari, F. Bonaccorso, V. Fal'Ko, K.S. Novoselov, S. Roche, P. Bøggild, S. Borini, et al., Science and technology roadmap for graphene, related two-dimensional crystals, and hybrid systems, Nanoscale 7 (11) (2015) 4598–4810.
[7] A. Zandiatashbar, R. Picu, N. Koratkar, Mechanical behavior of epoxy-graphene platelets nanocomposites, J. Eng. Mater. Technol. 134 (3) (2012) 031011.
[8] T. Kuilla, S. Bhadra, D. Yao, N.H. Kim, S. Bose, J.H. Lee, Recent advances in graphene based polymer composites, Prog. Polym. Sci. 35 (11) (2010) 1350–1375.
[9] P. Cataldi, I.S. Bayer, F. Bonaccorso, V. Pellegrini, A. Athanassiou, R. Cingolani, Foldable conductive cellulose fiber networks modified by graphene nanoplatelet-bio-based composites, Adv. Electron. Mater. 1 (12) (2015), 1500224–8.
[10] E.L. Papadopoulou, F. Pignatelli, S. Marras, L. Marini, A. Davis, A. Athanassiou, I.S. Bayer, Nylon 6, 6/graphene nanoplatelet composite films obtained from a new solvent, RSC Adv. 6 (8) (2016) 6823–6831.
[11] J.E. Mates, I.S. Bayer, M. Salerno, P.J. Carroll, Z. Jiang, L. Liu, C.M. Megaridis, Durable and flexible graphene composites based on artists' paint for conductive paper applications, Carbon 87 (2015) 163–174.
[12] V. Eswaraiah, S.S.J. Aravind, S. Ramaprabhu, Top down method for synthesis of highly conducting graphene by exfoliation of graphite oxide using focused solar radiation, J. Mater. Chem. 21 (19) (2011) 6800–6803.
[13] S. Park, R.S. Ruoff, Chemical methods for the production of graphenes, Nat. Nanotechnol. 4 (4) (2009) 217–224.
[14] B.Z. Jang, A. Zhamu, Processing of nanographene platelets (ngps) and ngp nanocomposites: a review, J. Mater. Sci. 43 (15) (2008) 5092–5101.
[15] R.J. Young, I.A. Kinloch, L. Gong, K.S. Novoselov, The mechanics of graphene nanocomposites: a review, Compos. Sci. Technol. 72 (12) (2012) 1459–1476.
[16] I. Zaman, T.T. Phan, H.-C. Kuan, Q. Meng, L.T.B. La, L. Luong, et al., Epoxy/graphene platelets nanocomposites with two levels of interface strength, Polymer 52 (7) (2011) 1603–1611.
[17] M.A. Rafiee, J. Rafiee, Z. Wang, H. Song, Z.-Z. Yu, N. Koratkar, Enhanced mechanical properties of nanocomposites at low graphene content, ACS Nano 3 (12) (2009) 3884–3890.
[18] H. Pang, L. Xu, D.-X. Yan, Z.-M. Li, Conductive polymer composites with segregated structures, Prog. Polym. Sci. 39 (11) (2014) 1908–1933.
[19] S. Chatterjee, F. Nafezarefi, N. Tai, L. Schlagenhauf, F. Nüesch, B. Chu, Size and synergy effects of nanofiller hybrids including graphene nanoplatelets and carbon nanotubes in mechanical properties of epoxy composites, Carbon 50 (15) (2012) 5380–5386.
[20] R. Mas-Balleste, C. Gomez-Navarro, J. Gomez-Herrero, F. Zamora, 2d materials: to graphene and beyond, Nanoscale 3 (1) (2011) 20–30.
[21] J.T. Choi, D.H. Kim, K.S. Ryu, H.-i. Lee, H.M. Jeong, C.M. Shin, et al., Functionalized graphene sheet/polyurethane nanocomposites: effect of particle size on physical properties, Macromol. Res. 19 (8) (2011) 809–814.
[22] K. Kalaitzidou, H. Fukushima, L.T. Drzal, Mechanical properties and morphological characterization of exfoliated graphite–polypropylene nanocomposites, Compos. Part A Appl. Sci. Manuf. 38 (7) (2007) 1675–1682.
[23] J. Du, H.-M. Cheng, The fabrication, properties, and uses of graphene/polymer composites, Macromol. Chem. Phys. 213 (10–11) (2012) 1060–1077.
[24] R. Verdejo, M.M. Bernal, L.J. Romasanta, M.A. Lopez-Manchado, Graphene filled polymer nanocomposites, J. Mater. Chem. 21 (10) (2011) 3301–3310.
[25] N. Yousefi, M.M. Gudarzi, Q. Zheng, X. Lin, X. Shen, J. Jia, et al., Highly aligned, ultralarge-size reduced graphene oxide/polyurethane nanocomposites: mechanical properties and moisture permeability, Compos. Part A Appl. Sci. Manuf. 49 (2013) 42–50.
[26] M. Fang, K. Wang, H. Lu, Y. Yang, S. Nutt, Covalent polymer functionalization of graphene nanosheets and mechanical properties of composites, J. Mater. Chem. 19 (38) (2009) 7098–7105.
[27] B. Das, K.E. Prasad, U. Ramamurty, C. Rao, Nano-indentation studies on polymer matrix composites reinforced by few-layer graphene, Nanotechnology 20 (12) (2009) 125705.
[28] J. Liang, Y. Huang, L. Zhang, Y. Wang, Y. Ma, T. Guo, et al., Molecular-level dispersion of graphene into poly (vinyl alcohol) and effective reinforcement of their nanocomposites, Adv. Funct. Mater. 19 (14) (2009) 2297–2302.
[29] J. Wang, X. Wang, C. Xu, M. Zhang, X. Shang, Preparation of graphene/poly (vinyl alcohol) nanocomposites with enhanced mechanical properties and water resistance, Polym. Int. 60 (5) (2011) 816–822.
[30] L. Ci, J. Bai, The reinforcement role of carbon nanotubes in epoxy composites with different matrix stiffness, Compos. Sci. Technol. 66 (3) (2006) 599–603.
[31] A.M. Pinto, J. Cabral, D.A.P. Tanaka, A.M. Mendes, F.D. Magalhães, Effect of incorporation of graphene oxide and graphene nanoplatelets on mechanical and gas permeability properties of poly (lactic acid) films, Polym. Int. 62 (1) (2013) 33–40.
[32] I. Zaman, H.-C. Kuan, J. Dai, N. Kawashima, A. Michelmore, A. Sovi, et al., From carbon nanotubes and silicate layers to graphene platelets for polymer nanocomposites, Nanoscale 4 (15) (2012) 4578–4586.
[33] K.A. Mkhoyan, A.W. Contryman, J. Silcox, D.A. Stewart, G. Eda, C. Mattevi, et al.,

Atomic and electronic structure of graphene-oxide, Nano Lett. 9 (3) (2009) 1058–1063.
[34] S. Pei, J. Zhao, J. Du, W. Ren, H.-M. Cheng, Direct reduction of graphene oxide films into highly conductive and flexible graphene films by hydrohalic acids, Carbon 48 (15) (2010) 4466–4474.
[35] H. Bai, C. Li, X. Wang, G. Shi, A ph-sensitive graphene oxide composite hydrogel, Chem. Commun. 46 (14) (2010) 2376–2378.
[36] H. Bai, K. Sheng, P. Zhang, C. Li, G. Shi, Graphene oxide/conducting polymer composite hydrogels, J. Mater. Chem. 21 (46) (2011) 18653–18658.
[37] X. Huang, X. Qi, F. Boey, H. Zhang, Graphene-based composites, Chem. Soc. Rev. 41 (2) (2012) 666–686.
[38] H. Kim, Y. Miura, C.W. Macosko, Graphene/polyurethane nanocomposites for improved gas barrier and electrical conductivity, Chem. Mater. 22 (11) (2010) 3441–3450.
[39] P. Steurer, R. Wissert, R. Thomann, R. Mülhaupt, Functionalized graphenes and thermoplastic nanocomposites based upon expanded graphite oxide, Macromol. Rapid Commun. 30 (4–5) (2009) 316–327.
[40] S. Sun, P. Wu, A one-step strategy for thermal-and ph-responsive graphene oxide interpenetrating polymer hydrogel networks, J. Mater. Chem. 21 (12) (2011) 4095–4097.
[41] Y. Xu, W. Hong, H. Bai, C. Li, G. Shi, Strong and ductile poly (vinyl alcohol)/graphene oxide composite films with a layered structure, Carbon 47 (15) (2009) 3538–3543.
[42] Y. Xu, Q. Wu, Y. Sun, H. Bai, G. Shi, Three-dimensional self-assembly of graphene oxide and dna into multifunctional hydrogels, ACS Nano 4 (12) (2010) 7358–7362.
[43] L. Zhang, Z. Wang, C. Xu, Y. Li, J. Gao, W. Wang, et al., High strength graphene oxide/polyvinyl alcohol composite hydrogels, J. Mater. Chem. 21 (28) (2011) 10399–10406.
[44] N. Jabeen, I. Majid, G.A. Nayik, F. Yildiz, Bioplastics and food packaging: A review, Cogent Food Agric. 1 (1) (2015) 1117749.
[45] A. Soroudi, I. Jakubowicz, Recycling of bioplastics, their blends and biocomposites: a review, Eur. Polym. J. 49 (10) (2013) 2839–2858.
[46] R. Wool, X.S. Sun, Bio-based Polymers and Composites, Academic Press, 2011.
[47] K.M. Zia, A. Noreen, M. Zuber, S. Tabasum, M. Mujahid, Recent developments and future prospects on bio-based polyesters derived from renewable resources: a review, Int. J. Biol. Macromol. 82 (2016) 1028–1040.
[48] S.W. Kim, H.M. Choi, Morphology, thermal, mechanical, and barrier properties of graphene oxide/poly (lactic acid) nanocomposite films, Korean J. Chem. Eng. 33 (1) (2016) 330–336.
[49] S.N. Raja, A.C.K. Olson, A. Limaye, K. Thorkelsson, A. Luong, L. Lin, et al., Influence of three-dimensional nanoparticle branching on the young's modulus of nanocomposites: effect of interface orientation, Proc. Natl. Acad. Sci. 112 (21) (2015) 6533–6538.
[50] F. Bonaccorso, A. Bartolotta, J.N. Coleman, C. Backes, 2D crystals-based functional inks, Adv. Mater (2016), http://dx.doi.org/10.1002/adma.201506410.
[51] A. Capasso, A.E. Del Rio Castillo, H. Sun, A. Ansaldo, V. Pellegrini, F. Bonaccorso, Ink-jet printing of graphene for flexible electronics: an environmentally-friendly approach, Solid State Commun. 224 (2015) 53–63.
[52] J. Hassoun, F. Bonaccorso, M. Agostini, M. Angelucci, M.G. Betti, R. Cingolani, M. Gemmi, C. Mariani, S. Panero, V. Pellegrini, B. Scrosati, An advanced lithium-ion battery based on a graphene anode and a lithium iron phosphate cathode, Nano Lett. 14 (8) (2014) 4901–4906.
[53] M. Boota, K. Hatzell, M. Alhabeb, E. Kumbur, Y. Gogotsi, Graphene-containing flowable electrodes for capacitive energy storage, Carbon 92 (2015) 142–149.
[54] K.E. Borchani, C. Carrot, M. Jaziri, Biocomposites of alfa fibers dispersed in the mater-bi type bioplastic: morphology, mechanical and thermal properties, Compos. Part A Appl. Sci. Manuf. 78 (2015) 371–379.
[55] D. Puglia, A. Tomassucci, J. Kenny, Processing, properties and stability of biodegradable composites based on mater-bi and cellulose fibres, Polym. Adv. Technol. 14 (11–12) (2003) 749–756.
[56] D. Bondeson, K. Oksman, Polylactic acid/cellulose whisker nanocomposites modified by polyvinyl alcohol, Compos. Part A Appl. Sci. Manuf. 38 (12) (2007) 2486–2492.
[57] M. Jonoobi, J. Harun, A.P. Mathew, K. Oksman, Mechanical properties of cellulose nanofiber (cnf) reinforced polylactic acid (pla) prepared by twin screw extrusion, Compos. Sci. Technol. 70 (12) (2010) 1742–1747.
[58] X. Liu, M. Dever, N. Fair, R. Benson, Thermal and mechanical properties of poly (lactic acid) and poly (ethylene/butylene succinate) blends, J. Environ. Polym. Degrad. 5 (4) (1997) 225–235.
[59] O. Martin, L. Averous, Poly (lactic acid): plasticization and properties of biodegradable multiphase systems, Polymer 42 (14) (2001) 6209–6219.
[60] O.C. Compton, S. Kim, C. Pierre, J.M. Torkelson, S.T. Nguyen, Crumpled graphene nanosheets as highly effective barrier property enhancers, Adv. Mater. 22 (42) (2010) 4759–4763.
[61] B.W. Chieng, N.A. Ibrahim, W.M.Z.W. Yunus, M.Z. Hussein, Poly (lactic acid)/poly (ethylene glycol) polymer nanocomposites: effects of graphene nanoplatelets, Polymers 6 (1) (2013) 93–104.
[62] E.M. Sullivan, Y.J. Oh, R.A. Gerhardt, B. Wang, K. Kalaitzidou, Understanding the effect of polymer crystallinity on the electrical conductivity of exfoliated graphite nanoplatelet/polylactic acid composite films, J. Polym. Res. 21 (10) (2014) 1–9.
[63] M. Mu, S. Osswald, Y. Gogotsi, K.I. Winey, An in situ raman spectroscopy study of stress transfer between carbon nanotubes and polymer, Nanotechnology 20 (33) (2009) 335703.
[64] B. Boonstra, A. Medalia, Effect of carbon black dispersion on the mechanical properties of rubber vulcanizates, Rubber Chem. Technol. 36 (1) (1963) 115–142.
[65] T. Prasse, L. Flandin, K. Schulte, W. Bauhofer, In situ observation of electric field induced agglomeration of carbon black in epoxy resin, Appl. Phys. Lett. 72 (22) (1998) 2903–2905.
[66] L. Jiang, T. Shen, P. Xu, X. Zhao, X. Li, W. Dong, et al., Crystallization modification of poly (lactide) by using nucleating agents and stereocomplexation, e-Polymers 16 (1) (2016) 1–13.
[67] Y. Cao, J. Feng, P. Wu, Preparation of organically dispersible graphene nanosheet powders through a lyophilization method and their poly (lactic acid) composites, Carbon 48 (13) (2010) 3834–3839.
[68] S. Wu, R.B. Ladani, J. Zhang, E. Bafekrpour, K. Ghorbani, A.P. Mouritz, et al., Aligning multilayer graphene flakes with an external electric field to improve multifunctional properties of epoxy nanocomposites, Carbon 94 (2015) 607–618.
[69] J.E. Mark, Physical Properties of Polymers Handbook, Springer, 2007.
[70] A. Lendlein, S. Kelch, Shape-memory polymers, Angew. Chem. Int. Ed. 41 (12) (2002) 2034–2057.
[71] T. Ramanathan, A. Abdala, S. Stankovich, D. Dikin, M. Herrera-Alonso, R. Piner, et al., Functionalized graphene sheets for polymer nanocomposites, Nat. Nanotechnol. 3 (6) (2008) 327–331.
[72] Q. Xue, C. Lv, M. Shan, H. Zhang, C. Ling, X. Zhou, et al., Glass transition temperature of functionalized graphene–polymer composites, Comput. Mater. Sci. 71 (2013) 66–71.
[73] T. Russell, Surface-responsive materials, Science 297 (5583) (2002) 964–967.